

Counting unique molecular identifiers in sequencing using a decomposable multitype branching process with immigration

Serik Sagitov^a and Anders Ståhlberg^{b,c,d}

^aMathematical Sciences, Chalmers University of Technology and University of Gothenburg, *serik@chalmers.se*

^bSahlgrenska Center for Cancer Research, Department of Laboratory Medicine, Institute of Biomedicine, University of Gothenburg, *anders.stahlberg@gu.se*

^cWallenberg Centre for Molecular and Translational Medicine, University of Gothenburg

^dRegion Västra Götaland, Sahlgrenska University Hospital, Department of Clinical Genetics and Genomics, Gothenburg, Sweden

May 16, 2022

Abstract

Detection of extremely rare variant alleles, such as tumour DNA, within a complex mixture of DNA molecules is difficult. Barcoding of DNA template molecules early in the next-generation sequencing library construction provides a way to identify and bioinformatically remove polymerase errors. During the PCR-based barcoding procedure consisting of t consecutive PCR-cycles, DNA molecules become barcoded by random nucleotide sequences. Previously, values 2 and 3 of t have been used, however even larger values of t might be relevant.

This paper proposes using a multi-type branching process with immigration as a model describing the random outcome of imperfect PCR-barcoding procedure, with variable t treated as the time parameter. For this model we focus on the expected numbers of clusters of molecules sharing the same unique molecular identifier.

1 Introduction

Massive parallel sequencing is applied in a wide range of applications within basic research and clinical applications. Numerous protocols and technologies are developed to accurately detect and quantify differences in sequences and detect variants. In cancer management, sequencing is applied in diagnostics and to identify mutations that can be targeted with specific therapies. Standard massive parallel sequencing can detect variants with frequencies down to the range of 1–5% [19, 20]. However, this sensitivity is not sufficient for several emerging applications. For example, detection of circulating tumor-DNA in liquid biopsies requires technologies that have the ability to detect variants with frequencies lower than 0.1% in clinically relevant samples [1, 6, 10]. The main source of sequencing noise is due to polymerase-induced errors that occur during library construction and sequencing [4].

To reduce sequencing noise, Unique Molecular Identifiers (UMIs), also known as DNA barcodes, can be used to enable ultrasensitive sequencing [12]. The UMIs typically consist of 8-12 randomized nucleotides that are experimentally attached to each target DNA molecule. The UMIs are introduced through a limited number of PCR cycles followed by a general amplification step (Figure 1). After sequencing, all reads with the same UMI can be tracked back to the original DNA molecule, allowing to control the polymerase-induced errors.

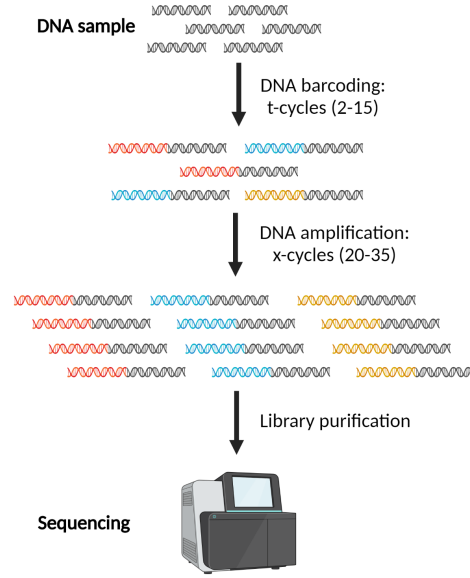


Figure 1: Overview of an ultrasensitive sequencing protocol. The experimental workflow consists of two PCR steps. In the first barcoding step, the UMIs are attached to target DNA molecules during t cycles of amplification. In the second adapter step, sequencing adapters are attached to barcoded DNA during x cycles of amplification. Typical numbers for the parameters t and x are shown. Finally, libraries are purified and sequenced.

Experimentally it is challenging to introduce UMIs, since randomized sequences easily produce non-specific PCR products. To address this challenge, several barcoding PCR cycles can be applied, which simplifies the experimental protocol [3, 18]. However, the number of different UMIs and their distribution is not easily estimated with increasing barcoding PCR cycles, limiting the use of UMIs in different applications.

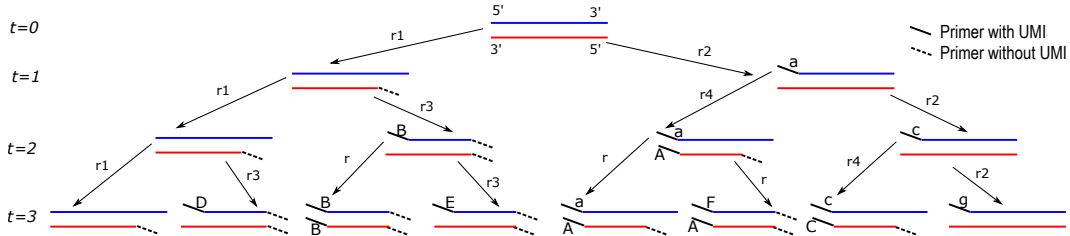


Figure 2: Schematic representation of three cycles barcoding PCR assuming 100% amplification rate. The two target DNA strands are shown in blue and red (sense and antisense, respectively). Forward primer with UMI and reverse primer are shown as the solid and dashed black segments. A single-stranded molecule needs primer sequences at both ends to be complete and used in downstream PCR. Capital letters mark complete molecules with different UMIs, while non-capitalized letters indicate incomplete molecules with different UMIs. The amplification rates r_1, r_2, r_3, r_4, r , in general, may differ from each other.

Figure 2 depicts the expected outcome of the first three cycles of PCR barcoding having 100% efficiency. For each double-stranded molecule, the upper segment represents a single-stranded molecule in the direction $5' \rightarrow 3'$ and the lower segment represents a single-stranded molecule in the direction $3' \rightarrow 5'$. The target double-stranded DNA molecule is placed at the top level, $t = 0$. The first PCR round produces two double-

stranded molecules shown at the level $t = 1$: the left pair consists of the target sense molecule plus the antisense molecule with a reverse primer, and the right pair consists of the target antisense molecule plus the sense molecule with a an attached UMI primer. All four single stranded molecules at $t = 1$ are incomplete with one generated UMI. The complete molecules start appearing at the level $t = 2$. With perfect PCR amplifications, the sizes of UMI clusters grow geometrically as shown in the left part of Table 1. For example at $t = 3$, as illustrated on Figure 2, there are six UMI clusters labelled by A, B, C, D, E, F, with B and D having size two, and A, C, E, F being singletons.

Table 1: The cluster numbers for t rounds of PCR duplications. On the left: all PCR duplications are successful. On the right: the summary of the outcome of Figure 3 with imperfect PCR duplications.

Cluster size	1	2	3	4	5	Total
$t = 2$	2	0	0	0	0	2
$t = 3$	4	2	0	0	0	6
$t = 4$	8	4	2	0	0	14
$t = 5$	16	8	4	2	0	30
$t = 6$	32	16	8	4	2	62

Cluster size	1	2	3	4	5	Total
$t = 2$	0	0	0	0	0	0
$t = 3$	1	0	0	0	0	1
$t = 4$	4	0	0	0	0	4
$t = 5$	4	2	0	0	0	6
$t = 6$	6	1	2	0	0	9

If the barcoding PCR amplifications are imperfect, then the outcome becomes random and the book-keeping of the barcodes produced by a larger number t of PCR cycles is at ruly challenging task. Figure 3 illustrates one such possible outcome summarised by the right part of Table 2. In particular, at $t = 6$, as shown in Figure 3, the UMIs A and D form clusters of size 3, the barcode B appears twice, and C, E, F, G, H, I are singletons.

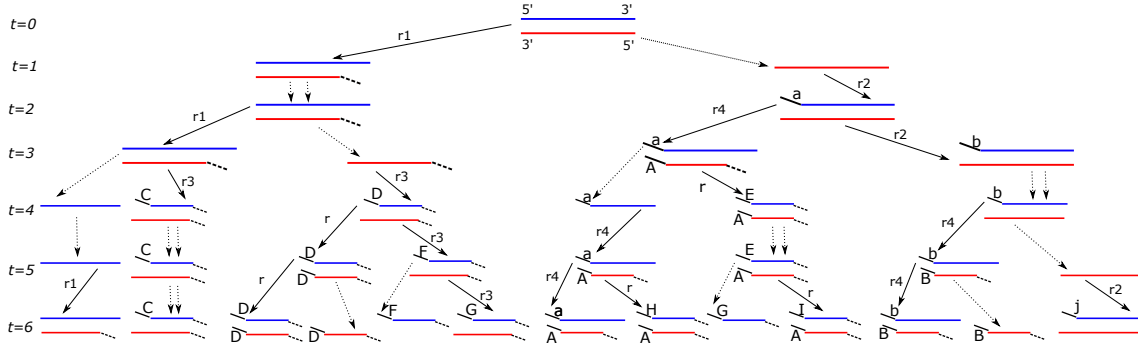


Figure 3: A possible output of the first six cycles for the barcoding PCR step with imperfect amplification. The failed PCR amplifications are marked by the dashed arrows and dashed double-arrows.

Despite the attempts to optimise the primers and reaction conditions, the PCR amplification rate are never close to 100%. Moreover, the amplification rate is dependent on both sequence context and sample quality. For example in the current setting, the original DNA molecules are often long, containing thousands or even millions base pairs. In addition, these molecules may have inhibitors attached to the DNA. These factors will reduce the amplification rate of the first molecules compared to the later formed DNA molecules. To address this phenomenon, we refer to five amplification rates (r_1, r_2, r_3, r_4, r) as indicated by Figures 2 and 3, assuming that

$$0 < r_1, r_2 \leq r_3, r_4 \leq r \leq 1. \quad (1)$$

This paper introduces a mathematical model for the outcome of the barcoding PCR experiment starting from a single double-stranded DNA molecule. Our stochastic model for counting the unique UMIs is built

upon an efficient bookkeeping system for the DNA barcoding procedure, presented in Section 2. We discriminate between six different types of single-stranded molecules emerging during the barcoding PCR procedure and introduce a Galton-Watson process [5] with four types of individuals and immigration describing the random process of reproduction of the single-stranded molecules see Section 3. This model leads to simple recursive formulas for the expected values for the number of clusters of a given size, see Section 4.

The use of branching processes as a stochastic model for counting of molecules in the repeated PCR amplification cycles is well established in the literature, see [5, 8, 11, 13, 14] and references therein. In [16] and [9] the branching process modelling is applied to the DNA amplification step of the UMI procedure, see Figure 1. However, to our knowledge, the branching processes were not used earlier for modelling the barcoding PCR procedure. The multitype Galton-Watson process with immigration of this paper is a special example of the multi-type Galton-Watson process with neutral mutations examined in [2].

Our main finding based on the analysis of the proposed multi-type Galton-Watson process is a simple pattern for the distribution of the cluster sizes. It says that for moderately large t , for any given set of parameters (r_1, r_2, r_3, r_4, r) , the increase of the cluster size by 1 reduces the number of clusters by half.

2 Tree-bookkeeping system for barcoding PCR

Figure 4 presents a convenient tree-graph view of the outcome of multiple rounds of perfect PCR duplications. Compared to the schematic representation of Figure 2, this alternative approach allows to neatly depict more than three PCR rounds using the same space. At any level t , the vertical branches (lineages) of the tree are connected pairwise thereby designating double-stranded molecules of Figure 2. We distinguish between six different types of lineages on the tree. At any level t there is exactly one target sense lineage labeled by 0, and one target antisense lineage labeled by 1. The other four type of lineages T_1, T_2, T_3, T_4 are defined by the following lineage generation rules:

$$0 \rightarrow T_1, \quad 1 \rightarrow T_2, \quad T_1 \rightarrow T_3, \quad T_2 \rightarrow T_4, \quad T_3 \rightarrow T_4, \quad T_4 \rightarrow T_3, \quad (2)$$

where

- the lineages 0, 1, T_1, T_2 represent incomplete molecules,
- the lineages T_3, T_4 represent complete molecules,
- newly generated lineages T_2 and T_3 represent molecules with a novel UMI,
- the lineages T_4 represent molecules that inherit the UMI of the parental molecule.

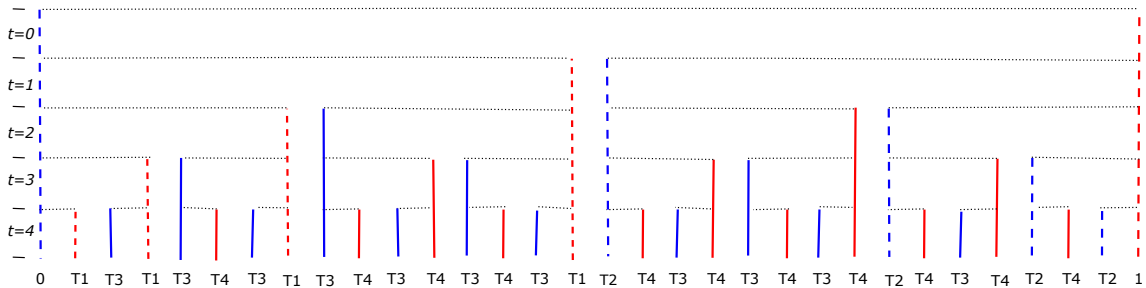


Figure 4: A tree-graph summary of the four rounds of perfect PCR duplications for DNA barcoding. Each vertical branch represents a molecule that once appeared persists over consecutive PCR rounds. The dashed and solid branches distinguish between the incomplete and complete molecules. Labels 0, 1, T_1, T_2, T_3, T_4 indicate different types of the molecules with and without UMIs, where the level t of the tree represents the cycle where the molecule is generated.

Let $Z_t^{(i)}$ stand for the number of the T_i -lineages at the level t , for $i = 1, 2, 3, 4$. Given

$$(r_1, r_2, r_3, r_4, r) = (1, 1, 1, 1, 1), \quad (3)$$

the evolution of the vector $(Z_t^{(1)}, Z_t^{(2)}, Z_t^{(3)}, Z_t^{(4)})$ is deterministic and in accordance with (2) satisfies the following recursions

$$\begin{aligned} Z_t^{(1)} &= Z_{t-1}^{(1)} + 1, & Z_t^{(2)} &= Z_{t-1}^{(2)} + 1, \\ Z_t^{(3)} &= Z_{t-1}^{(3)} + Z_{t-1}^{(1)} + Z_{t-1}^{(4)}, \\ Z_t^{(4)} &= Z_{t-1}^{(4)} + Z_{t-1}^{(2)} + Z_{t-1}^{(3)}, & t &\geq 1, \end{aligned}$$

with the initial condition

$$Z_0^{(1)} = Z_0^{(2)} = Z_0^{(3)} = Z_0^{(4)} = 0. \quad (4)$$

It is easy to see that $Z_t^{(1)} = Z_t^{(2)} = t - 1$, implying $Z_t^{(3)} = Z_t^{(4)}$. Thus

$$Z_t^{(3)} = 2Z_{t-1}^{(3)} + t - 2,$$

so that

$$Z_t^{(2)} + Z_t^{(3)} = 2(Z_{t-1}^{(2)} + Z_{t-1}^{(3)}) + 1,$$

yielding

$$Z_t^{(2)} + Z_t^{(3)} = 2^t - 1, \quad t \geq 0.$$

At any given level t , we split the set of complete lineages into clusters of lineages sharing the same UMI. According to our bookkeeping system, there are two different types of clusters:

- an x -cluster stems from a T_2 -lineage, it consists of the T_4 -lineages having the UMI of the stem lineage, with the stem lineage not being part of the cluster as it represents an incomplete molecule,
- a y -cluster stems from a T_3 -lineage, it consists of the stem lineage and the offspring T_4 -lineages having the UMI of the stem lineage.

Let $C_t(m)$ be the number of x -clusters and y -clusters of size m at the level t . Then

$$C_t := C_t(1) + \dots + C_t(t-1) \quad (5)$$

gives the total number of clusters at level t . Observe that given (3), we have

$$C_t = Z_t^{(2)} + Z_t^{(3)} - 1,$$

so that

$$C_t = 2^t - 2, \quad t \geq 1. \quad (6)$$

Furthermore, under (3), we get

$$C_{t+1}(1) = C_t + 2, \quad C_{t+1}(m+1) = C_t(m), \quad m \geq 2, \quad t \geq 1. \quad (7)$$

Here the first equality says that each existing cluster produces one novel UMI in addition to a new x -cluster and a new y -cluster. The second equality says that each existing cluster of size m becomes a cluster of size $m+1$. As a result,

$$C_t(m) = 2^{t-m}, \quad m \geq 1, \quad t \geq m+1, \quad (8)$$

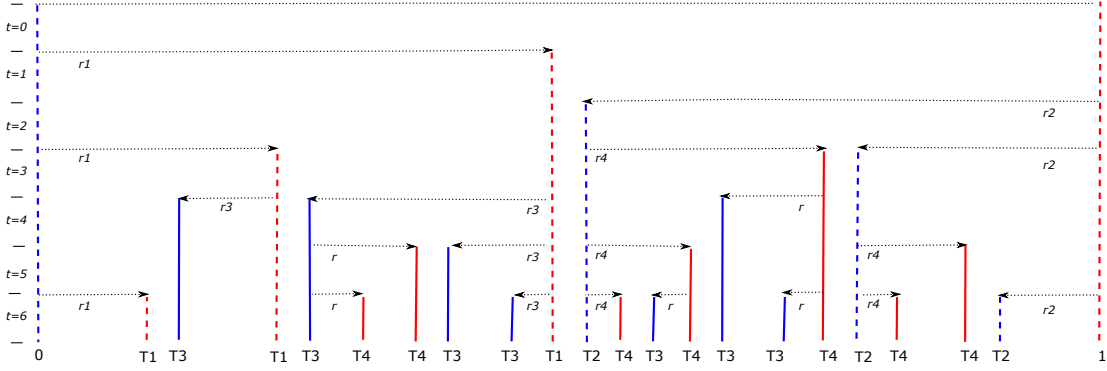


Figure 5: The tree view of the Figure 3. Depending on the corresponding type of the underlying DNA molecule, the five amplification rates r_1, r_2, r_3, r_4, r , are assigned to the corresponding horizontal arrows.

see Table 1. These relations imply an important rule of thumb saying that at any given t , the increase of the cluster size by 1 reduces the number of clusters by half. Indeed, by (8),

$$C_t(m)/C_t \rightarrow 2^{-m}, \quad m \geq 1, \quad t \rightarrow \infty. \quad (9)$$

If (3) does not hold, so that some PCR amplifications may fail, the cluster numbers $C_t(m), C_t$ become random. In the next section we give recursion relations for the corresponding mean values

$$c_t := E(C_t), \quad c_t(m) := E(C_t(m)), \quad 1 \leq m \leq t-1,$$

from which we will derive the following far-reaching extension of the deterministic relation (9):

$$c_t(m)/c_t \rightarrow 2^{-m}, \quad m \geq 1, \quad t \rightarrow \infty, \quad (10)$$

with the same limit irrespectively of the underlying amplification rates (r_1, r_2, r_3, r_4, r) , see Section 3. The approximation (10) may work very well already at $t = 10$, see Figure 6.

3 Multitype branching process with immigration

We are going to write $\xi \sim \text{Ber}(r)$ to say that a random variable ξ has a Bernoulli distribution with

$$P(\xi = 1) = r, \quad P(\xi = 0) = 1 - r.$$

Assuming that the amplification rates (r_1, r_2, r_3, r_4, r) satisfy (1), we restate (2) with

$$0 \rightarrow 0 + \xi_0 T_1, \quad T_1 \rightarrow T_1 + \xi^{(1)} T_3, \quad T_3 \rightarrow T_3 + \xi^{(3)} T_4, \quad (11)$$

$$1 \rightarrow 1 + \xi_1 T_2, \quad T_2 \rightarrow T_2 + \xi^{(2)} T_4, \quad T_4 \rightarrow T_4 + \xi^{(4)} T_3, \quad (12)$$

involving six random inputs

$$\xi_0 \sim \text{Ber}(r_1), \quad \xi_1 \sim \text{Ber}(r_2), \quad \xi^{(1)} \sim \text{Ber}(r_3), \quad \xi^{(2)} \sim \text{Ber}(r_4), \quad \xi^{(3)}, \xi^{(4)} \sim \text{Ber}(r).$$

We clarify these relations by referring to $T_3 \rightarrow T_3 + \xi^{(3)} T_4$, which says that a T_3 -lineage existing at any given level t , at the next level $t+1$ reproduces itself and may produce a new lineage of type T_4 .

The sequence of random vectors $(Z_t^{(1)}, Z_t^{(2)}, Z_t^{(3)}, Z_t^{(4)})_{t \geq 0}$ forms a Markov chain with the initial state (4). Treating relations (11) and (12) as the reproduction rules involving four types of individuals, we may

view this Markov chain as a multitype branching process with immigration [15]. This gives an example of a decomposable multitype branching process, which means that some pairs of types do not communicate, for example the type T_3 lineages may produce the type T_4 but not the types T_1 and T_2 . There are two sources of immigration generating new lineages of the types T_1 and T_2 at rates r_1 and r_2 respectively. The types T_1 and T_2 without directly communicating with each other, give arise to the types T_3 and T_4 respectively. The types T_3 and T_4 do reproduce each other, but not the types T_1 and T_2 . The reproduction rules (11) and (12) yield the following recursive relations

$$Z_t^{(1)} = Z_{t-1}^{(1)} + \xi_{t,0}, \quad Z_t^{(2)} = Z_{t-1}^{(2)} + \xi_{t,1}, \quad (13)$$

$$Z_t^{(3)} = Z_{t-1}^{(3)} + \sum_{j=1}^{Z_{t-1}^{(1)}} \xi_{t,j}^{(1)} + \sum_{j=1}^{Z_{t-1}^{(2)}} \xi_{t,j}^{(4)}, \quad Z_t^{(4)} = Z_{t-1}^{(4)} + \sum_{j=1}^{Z_{t-1}^{(2)}} \xi_{t,j}^{(2)} + \sum_{j=1}^{Z_{t-1}^{(3)}} \xi_{t,j}^{(3)}, \quad (14)$$

involving independent Bernoulli random values

$$\xi_{t,0} \sim \text{Ber}(r_1), \quad \xi_{t,1} \sim \text{Ber}(r_2), \quad \xi_{t,j}^{(1)} \sim \text{Ber}(r_3), \quad \xi_{t,j}^{(2)} \sim \text{Ber}(r_4), \quad \xi_{t,j}^{(3)}, \xi_{t,j}^{(4)} \sim \text{Ber}(r),$$

each indicating whether an underlying PCR amplification is successful or not.

The supercritical branching process $(Z_t^{(1)}, Z_t^{(2)}, Z_t^{(3)}, Z_t^{(4)})_{t \geq 0}$ could be described in terms of a single type branching process with a growing immigration. The specific reproduction rules (11) and (12) allow the types T_3 and T_4 to be treated as a single type, say T , such that the type T individuals produce $(1+r)$ offspring on average. In terms of the four-type branching process, the number Z_t of T -individuals at time t can be expressed as the sum

$$Z_t = Z_t^{(3)} + Z_t^{(4)},$$

and the Markov chain $(Z_t)_{t \geq 0}$ can be treated as a branching process with two sources immigration involving the types T_1 and T_2 as intermediates. By (14), the number of immigrants at time t is the sum

$$I_t = \sum_{j=1}^{Z_{t-1}^{(1)}} \xi_{t,j}^{(1)} + \sum_{j=1}^{Z_{t-1}^{(2)}} \xi_{t,j}^{(2)}$$

of two independent random variables having binomial distributions with parameters $(t, r_1 r_3)$ and $(t, r_2 r_4)$ respectively, so that

$$h_t(s) := \mathbb{E}(s^{I_t}) = (1 - r_1 r_3 + r_1 r_3 s)^t (1 - r_2 r_4 + r_2 r_4 s)^t, \quad 0 \leq s \leq 1, \quad t \geq 0. \quad (15)$$

The long term population size development of the supercritical branching processes with growing immigration is determined by the reproduction rate $(1+r)$ in that,

$$(1+r)^{-t} Z_t \rightarrow W \text{ in } L_2, \quad t \rightarrow \infty, \quad (16)$$

see Theorem 2b from Section 4 of [17]. Here, the limit W is a strictly positive random variable, whose Laplace transform

$$\mathbb{E}(e^{-\lambda W}) = \prod_{k=1}^{\infty} h_k(\lambda(1+r)^{-k})$$

is determined by the five amplification rates (r_1, r_2, r_3, r_4, r) in terms of the generating functions (15) and the limiting Laplace transform $\phi(\lambda)$ for the branching process without immigration, which satisfies the functional quadratic equation

$$\phi((1+r)\lambda) = (1-r)\phi(\lambda) + r\phi^2(\lambda).$$

The main concern of this paper is not the described decomposable multitype branching process per se, but certain functionals thereof, especially the total number of clusters C_t defined by (5) and

$$C_t(m) = X_t(m) + Y_t(m), \quad 1 \leq m \leq t-1,$$

where $X_t(m)$ is the number of x -clusters and $Y_t(m)$ is the number of y -clusters of size m at the level t . By (14), we have

$$Y_t(1) = \sum_{j=1}^{Z_{t-1}^{(1)}} \xi_{t,j}^{(1)} + \sum_{j=1}^{Z_{t-1}^{(4)}} \xi_{t,j}^{(4)} + \sum_{j \in \mathbb{Y}_{t-1}(1)} (1 - \xi_{t,j}^{(3)}). \quad (17)$$

Here, $\mathbb{Y}_t(m)$ is the set of T_3 -lineages whose barcodes are shared by exactly $(m-1)$ lineages of the type T_4 at the level t . Furthermore, again by (14), for $1 \leq m \leq t-1$,

$$X_t(m) = \sum_{j \in \mathbb{X}_{t-1}(m-1)} \xi_{t,j}^{(2)} + \sum_{j \in \mathbb{X}_{t-1}(m)} (1 - \xi_{t,j}^{(2)}), \quad (18)$$

$$Y_t(m) = \sum_{j \in \mathbb{Y}_{t-1}(m-1)} \xi_{t,j}^{(3)} + \sum_{j \in \mathbb{Y}_{t-1}(m)} (1 - \xi_{t,j}^{(3)}), \quad (19)$$

where $\mathbb{X}_t(m)$ is the set of T_2 -lineages whose barcodes are shared by exactly m lineages of the type T_4 at the level t , provided $m \geq 1$, while $\mathbb{X}_t(0)$ is the set of T_2 -singletons at the level t (by a T_2 -singleton we mean a T_2 -lineage that has not yet produced an offspring lineage).

Let $X_t(0)$ be the number of T_2 -singletons at the level t , so that for example, the outcome of Figure 5 produces

$$X_0(0) = X_1(0) = 0, \quad X_2(0) = X_3(0) = X_4(0) = 1, \quad X_5(0) = 0, \quad X_6(0) = 1.$$

Observe that due to (13) and (14),

$$X_t(0) = \xi_{t,1} + \sum_{j \in \mathbb{X}_{t-1}(0)} (1 - \xi_{t,j}^{(2)}). \quad (20)$$

Since

$$Z_t^{(2)} = X_t(0) + X_t(1) + \dots + X_t(t-1),$$

the total number of clusters at the level t equals

$$C_t = Z_t^{(2)} + Z_t^{(3)} - X_t(0). \quad (21)$$

In the expression (21) for the total number of clusters C_t , the dominating term is $Z_t^{(3)}$, which according to (16) is of order $(1+r)^t$. With this in mind, consider the first two moment of the total number of clusters C_t

$$c_t := E(C_t), \quad \sigma_t^2 := \text{Var}(C_t).$$

Relation (16) implies that both c_t and σ_t are growing proportionally to $(1+r)^t$ as $t \rightarrow \infty$.

4 The expected values

In this section we show first that

$$c_t = \alpha(1+r)^t + \alpha_1 t - \alpha_2 + \alpha_3(1-r_4)^t + \alpha_4(1-r)^t, \quad (22)$$

where

$$\alpha := \frac{r_1 r_3 + r_2 r_4}{2r^2}, \quad \alpha_1 := r_2(1 - r_4 r^{-1}), \quad \alpha_2 := r_1 r_3 r^{-2} + r_2 r_4^{-1}, \quad \alpha_3 := r_2 r_4^{-1}, \quad \alpha_4 := \frac{r_1 r_3 - r_2 r_4}{2r^2},$$

and then derive the main result (10) of this paper. Observe that $\alpha_4 = 0$ if $r_1 r_3 = r_2 r_4$, and in the deterministic case (3), relation (22) turns into (6).

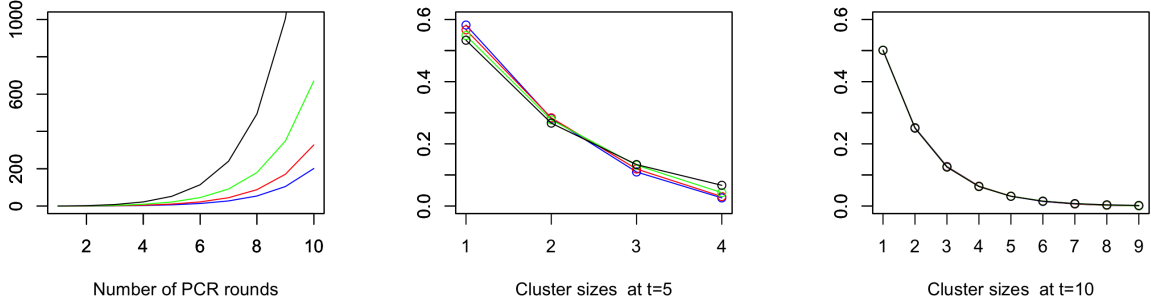


Figure 6: Left panel: the expected values of the total number of clusters. Middle ($t = 5$) and right ($t = 10$) panels show the plots of $z_t(m)/z_t$ over the cluster sizes $m = 1, \dots, t-1$. Different colours represent different sets of the parameters (r_1, r_2, r_3, r_4, r) : black $(1, 1, 1, 1, 1)$, green $(0.6, 0.6, 0.7, 0.8, 0.9)$, red $(0.4, 0.4, 0.6, 0.7, 0.9)$, blue $(0.3, 0.3, 0.4, 0.5, 0.9)$.

The proofs of (22) and (10), rely on the analysis of the expected values

$$z_t^{(i)} := E(Z_t^{(i)}), \quad x_t(m) := E(X_t(m)), \quad y_t(m) := E(Y_t(m)),$$

which due to (20), (18), (17), and (19), satisfy the following set of recursive relations

$$x_t(0) = r_2 + x_{t-1}(0)(1 - r_4), \quad (23)$$

$$y_t(1) = r_3 z_{t-1}^{(1)} + r z_{t-1}^{(4)} + y_{t-1}(1)(1 - r), \quad (24)$$

$$x_t(m) = x_{t-1}(m-1)r_4 + x_{t-1}(m)(1 - r_4), \quad 0 \leq m \leq t-1, \quad (25)$$

$$y_t(m) = y_{t-1}(m-1)r + y_{t-1}(m)(1 - r), \quad 0 \leq m \leq t-1. \quad (26)$$

Our results concerning the expected values are illustrated by Figure 6, on its right panel the four lines almost coincide demonstrating that asymptotic relation (10) works well already for $t = 10$.

PROOF OF (22). From (13) we obtain

$$z_t^{(1)} = r_1 + z_{t-1}^{(1)}, \quad z_t^{(2)} = r_2 + z_{t-1}^{(1)}, \quad z_0^{(1)} = z_0^{(2)} = 0,$$

so that $z_t^{(1)} = r_1 t$, $z_t^{(2)} = r_2 t$, and therefore by (14),

$$z_t^{(3)} = z_{t-1}^{(3)} + r_1 r_3 (t-1) + r z_{t-1}^{(4)},$$

$$z_t^{(4)} = z_{t-1}^{(4)} + r_2 r_4 (t-1) + r z_{t-1}^{(3)}.$$

Observe that

$$\begin{aligned} z_t^{(3)} + z_t^{(4)} &= (r_1 r_3 + r_2 r_4)(t-1) + (1+r)(z_{t-1}^{(3)} + z_{t-1}^{(4)}) \\ &= (r_1 r_3 + r_2 r_4) \sum_{j=1}^{t-1} (t-j)(1+r)^{j-1} = 2\alpha((1+r)^t - rt - 1) \end{aligned}$$

due to the relation

$$\sum_{j=1}^{t-1} (t-j)(1+r)^{j-1} = (1+r)^t \sum_{j=2}^t (j-1)(1+r)^{-j} = r^{-2}((1+r)^t - rt - 1).$$

On the other hand, we have

$$\begin{aligned} z_t^{(3)} - z_t^{(4)} &= (r_1 r_3 - r_2 r_4)(t-1) + (1-r)(z_{t-1}^{(3)} - z_{t-1}^{(4)}) \\ &= (r_1 r_3 - r_2 r_4) \sum_{j=1}^{t-1} (t-j)(1-r)^{j-1} = 2\alpha_4((1-r)^t + rt - 1), \end{aligned}$$

so that

$$\begin{aligned} z_t^{(3)} &= \alpha(1+r)^t - r_2 r_4 r^{-1} t - r_1 r_3 r^{-2} + \alpha_4(1-r)^t \\ z_t^{(4)} &= \alpha(1+r)^t - r_1 r_3 r^{-1} t - r_2 r_4 r^{-2} - \alpha_4(1-r)^t. \end{aligned}$$

Relation (23) yields

$$x_t(0) = r_2 r_4^{-1} (1 - (1-r_4)^t), \quad (27)$$

and since $c_t = z_t^{(2)} + z_t^{(3)} - x_t(0)$, see (21), we arrive at (22).

PROOF OF (10). By (24), we get a recursion

$$y_t(1) = \alpha r(1+r)^{t-1} - r_2 r_4 r^{-1} - \alpha_4 r(1-r)^{t-1} + y_{t-1}(1)(1-r),$$

which entails

$$\begin{aligned} y_t(1) &= \sum_{j=1}^{t-1} \left(\alpha r(1+r)^{t-j} - r_2 r_4 r^{-1} - \alpha_4 r(1-r)^{t-j} \right) (1-r)^{j-1} \\ &= \frac{1}{2} \alpha(1+r) \left((1+r)^{t-1} - (1-r)^{t-1} \right) - r_2 r_4 r^{-2} (1 - (1-r)^{t-1}) - \alpha_4 r(1-r)^{t-1} (t-1) \\ &= \frac{1}{2} \alpha(1+r)^t - r_2 r_4 r^{-2} - \alpha_4 r(1-r)^{t-1} (t-1) + \alpha_5 (1-r)^{t-1}, \end{aligned}$$

with $\alpha_5 := r_2 r_4 r^{-2} - \frac{1}{2} \alpha(1+r)$. Thus,

$$y_t(1) \sim \frac{1}{2} \alpha(1+r)^t, \quad t \rightarrow \infty.$$

Using this as the initiation step for the induction over m with help of recursion (26), we find

$$y_t(m) \sim 2^{-m} \alpha(1+r)^t, \quad m \geq 1, \quad t \rightarrow \infty.$$

This implies (10) in view of (22) and

$$c_t(m) = x_t(m) + y_t(m), \quad 1 \leq m \leq t-1,$$

since by (25) and (27), it is clear that $x_t(m) = o((1+r)^t)$.

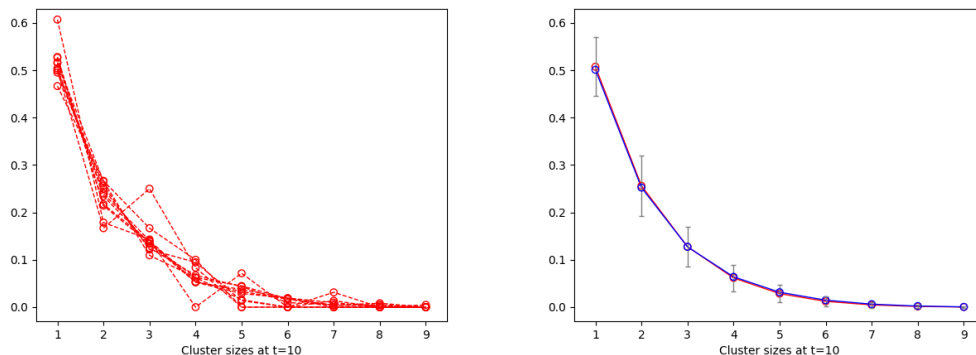


Figure 7: Simulation results for $Z_{10}(m)/Z_{10}$ and theoretical results for $z_{10}(m)/z_{10}$ over the cluster sizes $m = 1, \dots, 9$ assuming the amplification rates $(r_1, r_2, r_3, r_4, r) = (0.3, 0.3, 0.4, 0.5, 0.9)$. Left panel: ten individual simulation results. Right panel: the red line shows the average over 1 000 000 simulation results, the vertical intervals attached to the mean values are obtained from the the simulations as the mean \pm one standard deviation, the blue line depicts the theoretical values for $z_t(m)/z_t$ obtained in Section 3.

5 Discussion

We have shown that (9) holds in the simple case (3) when all PCR amplifications are successful. Under more general condition (1), we were able to establish (10), claiming a similar asymptotic result for the ratio of corresponding expected values. This theoretical result is illustrated by the right panel of Figure 6.

We hypothesise that given (1), a stronger version of (10),

$$E(C_t(m)/C_t) \rightarrow 2^{-m}, \quad m \geq 1, \quad t \rightarrow \infty \quad (28)$$

holds with the same limit irrespectively of the underlying amplification rates (r_1, r_2, r_3, r_4, r) . In [9], a simulation study based on our model was performed for the particular choice of the amplification rates $(r_1, r_2, r_3, r_4, r) = (0.3, 0.3, 0.4, 0.5, 0.9)$. These simulation results summarised in Figure 7 demonstrate that approximation (28) may work well even for the moderate values of t .

Acknowledgements

We are grateful to professor Peter Jagers for bringing us together and for fruitful discussions.

This research was partially funded by Region Västra Götaland, Sweden; Swedish Cancer Society (20-1098); Swedish Research Council (2020-01008); Swedish Childhood Cancer Foundation (MTI2019-0008 and 2020-0007); the Swedish state under the agreement between the Swedish government and the county councils, the ALF-agreement (ALFGBG-965065); Sweden's Innovation Agency and the Sjöberg Foundation.

References

- [1] Andersson, D., Kristiansson, H., Kubista, M., Ståhlberg, A. *Ultrasensitive circulating tumor DNA analysis enables precision medicine: experimental workflow considerations*. Expert Rev. Mol. Diagn. 21 (2021) 299–310.
- [2] Bertoin J. *The structure of the allelic partition of the total population for Galton-Watson processes with neutral mutations*. Ann. Probab. 37 (2009) 1502–1523.
- [3] Cohen, J.D. et al. *Detection and localization of surgically resectable cancers with a multi-analyte blood test*. Science 359 (2018) 926–930.

- [4] Filges, S., Yamada, E., Ståhlberg A, Godfrey T.E. *Impact of polymerase fidelity on background error rates in next-generation sequencing with unique molecular identifiers/barcodes*. Sci. Rep. 9 (2019) 3503.
- [5] Haccou, P., Jagers, P., Vatutin, V. *Branching processes: variation, growth, and extinction of populations*. Cambridge Studies in Adaptive Dynamics, Cambridge University Press (2005).
- [6] Ignatiadis, M., Sledge, G.W., Jeffrey, S.S. *Liquid biopsy enters the clinic—Implementation issues and future challenges*. Nat. Rev. Clin. Oncol. 18 (2021) 297–312.
- [7] Jagers, P. *Branching processes with biological applications*. John Wiley (1975).
- [8] Jagers, P., Klebaner, F.C. *Random variation and concentration effects in PCR*. J. Theoret. Biol. 224 (2003) 299–304.
- [9] Gu, Y., Zhan, H. *Counting unique molecular identifiers using PCR-branching models*. Master degree thesis, Chalmers University of Technology (2022).
- [10] Heitzer, E., Haque, I.S., Roberts, C.E., Speicher, M.R. *Current and future perspectives of liquid biopsies in genomics-driven oncology*. Nat. Rev. Genet. 20 (2019) 71–88.
- [11] Kimmel, M., Alexrod, D. E. *Branching processes in biology*. Interdisciplinary Applied Mathematics Vol. 19 (2002).
- [12] Kinde, I., Wu, J., Papadopoulos, N., Kinzler, K.W., Vogelstein, B. *Detection and quantification of rare mutations with massively parallel sequencing*. Proc. Natl. Acad. Sci. USA 108 (2011) 9530–9535.
- [13] Krawczak, M., Reiss, J., Schmidtke, J., Rösler, U. *Polymerase chain reaction: replication errors and reliability of gene diagnosis*. Nucleic Acids Res. 17 (1989) 2197–2201.
- [14] Lalam, N. *Estimation of the reaction efficiency in polymerase chain reaction*. J. Theor. Biol. 242 (2006) 947–953.
- [15] Mode, C.J. *Multitype branching processes: theory and applications*. American Elsevier (1970).
- [16] Pflug, F.G., von Haeseler, A. *TRUmiCount: correctly counting absolute numbers of molecules using unique molecular identifiers*. Bioinformatics 34 (2018) 3137–3144.
- [17] Rahimov, I. *Homogeneous branching processes with non-homogeneous immigration*. Stochastics and Quality Control 36 (2021) 165–183.
- [18] Ståhlberg, A., Krzyzanowski, P.M., Jackson, J.B., Egyud, M., Stein, L., Godfrey, T.E. *Simple, multiplexed, PCR-based barcoding of DNA enables sensitive mutation detection in liquid biopsies using sequencing*. Nucleic Acids Res. 44 (2016) 105.
- [19] Stead, L.F., Sutton, K.M., Taylor, G.R., Quirke, P., Rabbitts, P. *Accurately identifying low-allelic fraction variants in single samples with next-generation sequencing: Applications in tumor subclone resolution*. Hum Mutat, 34 (2013) 1432–1438.
- [20] Xu, H., DiCarlo, J., Satya, R.V., Peng, Q., Wang, Y. *Comparison of somatic mutation calling methods in amplicon and whole exome sequence data*. BMC Genomics 15 (2014) 244.